Systematic Evaluation of the Immune Environment of Small Intestinal Neuroendocrine Tumours

Clare Vesely[1*], Yien Ning Sophia Wong[1, 2*], Alexa Childs[1,3], Ayse U. Akarca[1], Pawan Dhami[1], Heli Vaikkinen[1], Lucia Conde[1], Javier Herrero[1], Olagunju Ogunbiyi[3], Amir Gander[3], Tu Vinh Luong[3], Chrissie Thirlwell[1,4], Martyn Caplin[3], Christos Toumpanakis[3], Karl Peggs[1,2], Sergio A. Quezada[1,2], Teresa Marafioti[1], Tim Meyer[1,3]

* These authors have contributed equally to this work

[1]UCL Cancer Institute, UCL, London, WC1E 6DD, UK. [2] Cancer Immunology Unit, Research Department of Haematology, UCL Cancer Institute, UCL, London, WC1E 6DD, UK. [3] Royal Free Hospital, Pond Street, London NW3 1JP, UK. [4] The University of Exeter Medical School

Corresponding author: Professor Tim Meyer, UCL Cancer Institute, University College London. 72 Huntley Street, London WC1E 6DD, email; t.meyer@ucl.ac.uk Tel; +44 207 679 6731.

Running Title: Immune environment of SI neuroendocrine tumours

Keywords: T cells, immunotherapy, neuroendocrine tumor, Treg, small intestine

Conflict of Interest: none

Word Count: 5466

Tables: 1, Figures: 5, Supplementary Figures: 9, Supplementary Tables: 1

Statement of translational relevance

Most patients with small intestinal neuroendocrine tumours (siNET) present with advanced, metastatic disease. Current standard therapies consistently offer objective response rates of less than 20% and trials of immune checkpoint inhibitors to date, have failed to improve on this. Here, we have performed a detailed analysis of the immune microenvironment in siNET in order to inform a rational approach for targeting the immune system in this tumour. We demonstrated that effector tumour infiltrating lymphocytes had a significantly higher expression of checkpoint molecules including high levels of PD-1 expression in the tumour microenvironment compared to the periphery and that PD-1 is frequently co-expressed with other checkpoint molecules including CTLA-4 and ICOS. Moreover, immunohistochemistry revealed an exclusion immune phenotype with a higher number of T cells peri-tumourally compared to intra-tumourally. These finding suggest that combination therapy will be required to target multiple checkpoints and strategies to reverse the immune exclusion phenotype need to be explored.

ABSTRACT

Background: The immune tumour microenvironment and the potential therapeutic opportunities for immunotherapy in small intestinal neuroendocrine tumours (siNET) have not been fully defined.

Methods: Herein, we studied 40 patients with primary and synchronous metastatic siNETs , and matched blood and normal tissue obtained during surgery. We interrogated the immune checkpoint landscape using multi-parametric flow cytometry. Additionally, matched FFPE tissue was obtained for multi-parametric immunohistochemistry (IHC) to determine the relative abundance and distribution of T-cell infiltrate. Tumour mutational burden (TMB) was also assessed and correlated with immune infiltration.

Results: Effector tumour infiltrating lymphocytes had a higher expression of PD-1 in the tumour microenvironment compared to the periphery. Additionally, $CD8^+$ tumour infiltrating lymphocytes had a significantly higher co-expression of PD-1/ICOS and PD-1/CTLA-4 and higher levels of PD-1 expression compared to normal tissue. IHC revealed that the majority of cases have ≤10% intratumoural T cells but a higher number of peritumoural T cells, demonstrating an "exclusion" phenotype. Finally, we confirmed that siNETs have a low TMB compared to other tumour types in the TCGA database but did not find a correlation between TMB and CD8/Treg ratio.

Conclusions: Taken together, these results suggest that a combination therapy approach will be required to enhance the immune response, using PD-1 as a checkpoint immunomodulator backbone in combination with other checkpoint targeting molecules (CTLA-4 or ICOS), or with drugs targeting other pathways to recruit "excluded" T cells into the tumour microenvironment to treat patients with siNETs.

INTRODUCTION

An adaptive immune response is initiated through antigen recognition by a T cell receptor (TCR) on a T cell, but the final quality and amplitude of the immune response elicited is ultimately dictated by an additional layer of checkpoint signalling (1). This signalling is regulated through a balance of co-inhibitory and co-stimulatory checkpoint molecules found on the cell surface. These immune checkpoints are needed under normal physiological conditions in preventing autoimmunity in the form of "self-tolerance". One mechanism by which tumours evade immune surveillance is by dysregulation of these immune checkpoint molecules. There is now a myriad of immune checkpoint inhibitors (CPIs) in various stages of clinical development that act by targeting checkpoint molecules, in order to tip the immune response back toward tumour destruction (1-3).

This approach has been effectively used to target the checkpoint molecule Programmed Cell Death-1 (PD-1) and its ligand, Programmed Cell Death Ligand-1 (PD-L1) with therapeutic antibodies including nivolumab, pembrolizumab, atezolizumab and durvalumab, in a range of advanced solid malignancies (4-6). Moreover, the monoclonal antibody, ipilimumab, which targets the Cytotoxic T Lymphocyte Antigen-4 (CTLA-4) is the first drug in 30 years to improve survival in metastatic melanoma, a disease with previously poor survival outcomes and minimal treatment options (7). Critically, these patients with metastatic melanoma who respond can derive long-term, durable remissions, particularly to combination CPIs that target different checkpoints (8).

Neuroendocrine tumours are a diverse group of neoplasms that arise from enterochromaffin cells located throughout the body, but most commonly within the GI

tract, pancreas and lungs. They are remarkable for their heterogeneity in terms of biology, clinical behaviour and prognosis, with a median survival of approximately 10 months in patients with metastatic high-grade tumours, as compared to 16.2 years in low grade disease (9). Not only do the anatomical subgroups have distinct molecular profiles, but they also respond differently to therapies including cytotoxic chemotherapy, receptor tyrosine kinase inhibitors and checkpoint inhibitors. For this reason, and to reduce the impact of confounding factors, we confined our analysis to a well-defined anatomical subgroup.

The majority of patients with small intestinal neuroendocrine tumours (siNET) present with advanced metastatic disease which is not amenable to curative surgery, and a range of systemic therapies may be offered including somatostatin analogues (10), cytotoxic chemotherapy (11), the mTOR inhibitor everolimus (12) and peptide receptor radionuclide therapy (PRRT) (13). Objective response rates to these treatments are consistently less than 20% and there is a need to develop more effective therapies with more sustained tumour control rates. Immunotherapeutic approaches have been successfully applied to high grade neuroendocrine tumours including Merkel cell carcinoma, and both avelumab and pembrolizumab have been approved in this indication. However, efficacy data from small cohorts of gastrointestinal NET has been disappointing with 2% response rate reported for pembrolizumab (14), 3.1% for spartalizumab (15, 16) and no responses reported for durvalumab and tremilimumab. The majority of GI NET are low grade and data from the combination of ipilimumab plus nivolumab demonstrate better response rates in high grade tumours at 44% compared to 0% in low grade tumours (17).

Whilst there have been a number of studies that have evaluated PD1 or PD-L1 expression in siNETs (18), a comprehensive analysis of the immune checkpoint profile in siNET has not been reported. We hypothesize that a deeper understanding of the molecular landscape might provide a rationale for the development of immunotherapy in siNET and in this study have performed a systematic analysis of the immune microenvironment in 40 patients with siNET.

MATERIALS AND METHODS

Patients and samples

Eligible patients were required to have histologically confirmed NET of small intestinal origin. Data were collected on age, gender, primary site and grade according to the European Neuroendocrine Tumour Society (ENETS)/WHO guidelines (19). This study was conducted in accordance with the Declaration of Helsinki, was approved by the Local Ethics Committee (IRAS REC reference 15/LO/1567) and all participants were required to provide written informed consent. Peripheral blood samples were collected into a 10 mL EDTA tube. Peripheral blood mononuclear cells (PBMCs) were isolated by density-gradient centrifugation with Ficoll-Paque PLUS (GE Healthcare). Isolated live cells were frozen at -80°C and stored until analysis. Fresh tissue samples were dissected surgically, and both tumour regions and normal adjacent were defined macroscopically by a pathologist and collected in serum-free RPMI culture medium. Single-cell suspensions were prepared by mechanical disruption of tissue using a scalpel and digestion with with a mixture of 0.2 mg/mL DNase (and 0.3 mg/mL Liberase TL or 2.5 mg/mL Collagenase in serum-free RPMI for 1 hour on a GentleMACS Dissociator (Miltenyi Biotec). Samples were filtered through a 70 µm cell strainer, and leukocytes were enriched by density-gradient centrifugation with Ficoll-Paque PLUS (GE Healthcare). Finally, the isolated cells were frozen at -80°C for 24hs and then cryogenically stored until analysis.

Flow cytometry

Acquisition was performed with a BD LSR II Fortessa (BD Biosciences). The following antibodies and fluorescent labels were used to stain samples for T cell analysis: from

Biolegend; PD-1-BV605 (EH12.2H7), CD3-BV785 (OKT3), CTLA-4-APC (L3D10), ICOS-PE/Cy7 (C398.4A), OX40-PE/Cy7 (Ber-ACT35), Streptavidin-APC and 4-1BB-PE (4B4-1): from BD Biosciences; CD8-V500 (SK1), and TIM-3-BV650 (7D3); from eBioscience, FoxP3-PerCP-Cy5.5 (PCH101), CD4-AF700 (OKT-4), TIGIT-PE (MBSA43) and fixable viability dye-e780: and GITR-Biotin (DT5D3) from Miltenyi Biotec. Intranuclear staining of FoxP3 and Ki67 was performed using the FoxP3/Transcription Factor Staining Buffer Set (eBioscience) and FITC Mouse Anti-Ki-67 Set (BD Biosciences). Data were analysed with FlowJo v.10.6.0 (BD Biosciences) and samples were required to have >20 cells in all subsets to be eligible for analysis. For co-expression data, samples with > 500 viable CD3 cells were taken forward for analysis. Samples were concatenated and analysed using FlowJo plugins (https://flowjo.com/exchange/#/), namely: Downsample (v.3.2), UMAP (v2.2), and FlowSOM (v2.6).

Multiplex immunohistochemistry

3μm tissue sections were cut and transferred onto poly-l-lysine–coated slides, dewaxed in two changes of xylene and rehydrated in a series of graded alcohols. Sections were stained with H&E according to standard procedures. Primary antibodies used were anti-CD4 (clone: SP35; dilution: 1/50 (3.1 μg/ml); Abcam Plc.) (20), anti-CD8 (clone: SP239; dilution: 1/100 (5.0 μg/ml); Abcam Plc.), anti-FOXP3 (clone: 236A/E7; dilution: 1/100 (99.8 μg/mL); a kind gift from Dr G Roncador, CNIO, Madrid, Spain) (21, 22) and anti-Cytokeratin (clone:AE1/AE3 ; dilution: 1/100 (17.1 μg/mL); Agilent Technologies Inc.,). Single immunohistochemistry was carried out using the automated platforms BenchMark Ultra (Ventana/Roche) and the Bond-III Autostainer (Leica Microsystems) according to a protocol described elsewhere (23, 24) (Figure S1). To establish optimal staining conditions (i.e. antibody dilution and incubation

time, antigen retrieval protocols, suitable chromogen) each antibody was tested and optimized on sections of human reactive tonsil, used as positive control. Multiplex immunohistochemistry (IHC) was carried out using a protocol described previously (25). Briefly, pre-treated sections were incubated 30 min with the first primary antibody at room temperature and the then developed with peroxidase-based detection system (Envision System; Agilent Technologies, Inc.) to visualise antibody-binding site. The following step included the second antibody incubation, and its visualization with an alkaline phosphatase kit (Dako REAL Detection System; Agilent Technologies, Inc.). Lastly, both steps were repeated for the application of third and the fourth antibodies. After staining, samples were washed in buffers and distilled water and mounted in Apathys mounting medium (TCS Biosciences Ltb). Specificity of the staining was assessed by a haematopathologist (TM) according to the conventional principles of antibodies validation measuring the specificity of the protein cellular localization, the sensitivity of the antibody staining was controlled by using different antibodies concentration. Slides were scanned using the NanoZoomer Digital Pathology System C9600 (Hamamatsu).

IHC analysis

Immune cells from scanned images were analysed with using QuPath 0.1.2 (open-source software, Bankhead, P *et al*. 2017 Scientific Reports). The T cells analysis strategy was designed to approximate recommendations made by Obeid *et al*. 2017 to sample multiple small areas encompassing 3 mm^2 within the central tumour avoiding areas of dense lymphoid aggregates (DLA) and away from the periphery and invasive margin (26). For this reason, we selected 6 central tumour regions of 500 μm^2 avoiding areas of DLA to encompass a total area of 3 mm^2. Cytokeratin was used as tumour marker to identify the

tumour area. Each case was scored first to assess the distribution of the inflammatory cells within the intra and peritumoral area and we selected 6 regions as representative of the trend of immune cells distribution. Where multiple lesion sites were present, we spread our sampling areas between the major sites to as best as possible represent the whole tumour. The number of cells were manually counted using NDP.view2 viewing software (Hamamatsu).

Statistical analysis

Statistical analyses were done with GraphPad Prism 7.03 (GraphPad Software); p values were calculated using the Kruskal-Wallis analysis of variance and Dunn's post-hoc test with error bars represent mean values with SEM, unless otherwise indicated (ns = p > 0.05; *p % 0.05; **p % 0.01; ***p % 0.001; ****p % 0.0001).

Genomic DNA extraction

96 samples from the 40 patients, including 56 formalin fixed paraffin embedded (FFPE) tumour tissue tumours and 40 matching controls (9 FFPEs, 31 fresh-frozen) were sent for exome sequencing. DNA was extracted from 10 µm sections of FFPE tumour tissue using the DNAstorm FFPE DNA Isolation Kit (CELLDATA) according to manufacturers' instructions. Matched germline DNA was extracted from 1mL peripheral blood using the DNAeasy Blood & Tissue Kit (QIAGEN) following the manufacturers' protocol. DNA concentrations were measured using the NanoDrop-1000 Spectrophotometer (NanoDrop) and Qubit 2.0 Fluorometer (Invitrogen).

Exome-seq library preparation and sequencing

DNA samples were quantified using either Qubit dsDNA High Sensitivity or Qubit dsDNA Broad Range kit (Invitrogen). DNA quality was assessed, and a DNA integrity number (DIN) assigned using Agilent Tapestation (Agilent). Exome-Seq libraries for the samples were generated using Roche SeqCap EZ HyperCap Workflow, using KAPA HyperPlus library preparation kit . 150 ng of genomic DNA for fresh frozen, 300 ng for FFPE samples (DIN > 3), and 1000 ng for FFPE samples (DIN < 3) was used as starting input for library preparation. AMPure XP beads (Beckman Coulter) were used to perform double sided size selection of the libraries according to the Roche SeqCap EZ HyperCap workflow (Roche). Libraries were assessed for average fragment size and quality using Agilent Bioanalyzer DNA 1000 chips and quantified using KAPA Library quantification kit for Illumina platforms (Roche). Roche SeqCap EZ MedExome Enrichment kit and exome panel were used according to Roche SeqCap EZ HyperCap workflow to perform exome capture.

Post amplification, the Exome-Seq libraries were assessed for average insert size using Agilent Bioanalyzer DNA 1000 chips and quantified using KAPA Library quantification kit for Illumina platforms (Roche).The molar concentration of the libraries was determined using the following formula:

$$\frac{(\text{concentration in ng}/\mu\text{l})}{(660\ \text{g/mol} \times \text{average library size in bp})} \times 10^6 = \text{concentration in nM}$$

The Exome-Seq libraries were manually normalised to 10 nM and combined to generate 8 library pools which were sequenced on Illumina HiSeq 2500 platform, utilising two High

Output flow cells, with cluster generation performed on Illumina cBot instrument to obtain the required number of reads needed.

Genomic analysis

FastQ files were processed with the SciLifeLab/Sarek v2.3.FIX1 pipeline (27). Specifically, reads were aligned against GRCh38 using BWA v0.7.17 and processed using GATK v4.1.1.0. The coverage in tumour samples ranged from 36X to 142X (median 74X) and in controls from 25X to 76X (median 54X). Somatic variant calling was performed with mutect2 following the GATK (v4.1.9.0) best practices, using a panel of normal created from the 40 control samples used in the analysis, and with the mutect2 --tumor-lod-to-emit argument (TLOD threshold) set to 7.3. The funcotator tool from GATK v4.1.9.0 was used to annotate the variants according to their effect on the canonical transcript, and the maftools R package was used to create mutation summary plots.

Initial analysis pointed to an obvious excess of C>T mutations, consistent with known artefacts in FFPE samples resulting from deamination during formalin fixation. To decrease the amount of C>T false positives and improve the quality of the callset, we used a higher TLOD threshold for C>T mutations and filtered out C>T mutations of low allele frequency, common gnomad variants (AF>0.0001), low-confidence variants (n_alt_count > 1 | t_depth < 30 | t_alt_count <= 5), and variants in the top-20 Frequently Mutated Genes (FLAGS) (28).

Data availability statement

The data generated in this study are available within the article and its supplementary data files.

RESULTS

Patient cohort

Fresh tissue and blood were collected from 40 patients with a confirmed diagnosis of siNET from the Royal Free Hospital, London, between September 2015 and June 2018. Thirty-nine samples were collected from patients undergoing surgical resections and one was collected from a patient undergoing a tissue biopsy. The median age was 62 with range, 27-85 years. Metastatic disease was present at the time of the procedure in 75% (n=30). Overall, 65% (n=26) had Grade 1 disease, 32.5% (n= 13) Grade 2 and 2.5% (n=1) Grade 3. At the time of sample collection 60% (n=24) of patients were receiving somatostatin analogues (SSA) and one had undergone Peptide Receptor Radionuclide Therapy (PRRT), the rest were treatment naïve (Table 1). In each case, fresh tissue was collected from the tumour (n=25) and, for those undergoing surgical resection, normal control tissue was also sampled from a distal part of the resection specimen where possible (n=22). Normal tissue was sampled at least 5cm from the macroscopically visible tumour by an experienced pathologist. Metastatic tumour was also sampled where feasible (n=23). Peripheral blood was collected concurrently at time of surgery; one sample for genomic DNA extraction and a second for immune cell profiling. Formalin fixed paraffin embedded (FFPE) tissue was also obtained for immunohistochemistry (IHC) and tumour genomic DNA extraction.

Evaluation of T cells subsets indicates that siNET tumour have a lower effector T cells to regulatory T cells ratio than normal tissue in CD8 and PBMC in CD4eff.

Isolated lymphocytes were analysed by flow cytometry to define T cell ($CD3^+$) subpopulations; $CD8^+$ cytotoxic T cells, $CD4^+$ $FoxP3^-$ effector T cells (CD4eff) and $CD4^+$ $FoxP3^+$

regulatory T cells (Tregs) (Figure S2). The samples included PBMCs (n=32), normal bowel tissue (n=35), primary tumour tissue (n=32) and metastases (consisting mainly of mesenteric masses (n=23) or metastatic lymph nodes (n=2)). The ratio of the effector T cells to Tregs for each tissue compartment was calculated to evaluate the balance of the immune environment in these compartments (Figure 1A). There was a significantly higher CD8/Treg ratio in the normal bowel tissue compared to the tumour tissues in both primary and metastatic ($p = 0.005$ and $p = 0.0046$ respectively), while there was a significantly higher CD4eff/Treg ratio in PBMC compared to the tumour tissue, both primary and metastatic ($p = 0.0073$ and 0.0255 respectively). This suggests that the siNETs have a more inhibitory immune tumour microenvironment with lower effector/Treg ratio, whether primary or metastases, compared to normal tissue and PBMC.

Single immune checkpoint molecules are expressed highly on regulatory T cells and lower in PBMC in siNETs

T cell subsets from normal tissue, PBMC, and tumours from primary and metastatic sites were stained for checkpoint molecules and their expression analysed by flow cytometry. To determine the balance of checkpoint molecule expression, cells were stained for co-inhibitory checkpoint molecules; CTLA-4, PD-1, TIM-3 and TIGIT and co-stimulatory checkpoint molecules; ICOS, 4-1BB, OX-40 and GITR. We also evaluated activation and proliferation markers including Ki67, Granzyme B (GzmB) and CD25. Ki67 is an intracellular marker for proliferation, GzmB is a serine protease most commonly found in cytotoxic T cells and natural killer cells (29), while CD25 is present on activated T cells (30).

For all checkpoint molecules, levels of expression on the Tregs were significantly higher than on the effector T cells (both $CD8^+$ and CD4eff) for normal tissue, primary and metastatic tumour and PBMCs (Figure 1B; Figure S3). The only exception was TIM-3 and OX-40 expression on PBMCs for which there was no significant difference between the $CD8^+$ or CD4eff respectively and the Tregs. For all of the other checkpoint molecules, there was a significant difference between both the effector T cells and Tregs in the PBMCs. We next explored whether there were differences between the single checkpoint molecule expression in the tissue types. PD-1 and CTLA-4 were significantly expressed on $CD8^+$ cells in tumours compared to PBMC and normal tissues, while for $CD8^+$ TIGIT was significantly higher in PBMC. TIM-3 and TIGIT was significantly expressed on CD4eff in metastatic tumours compared to the other tissue types, while PD-1 and CTLA-4 expression were significantly lower in PBMC. PD-1, TIM-3, OX-40 and GITR expression were significantly lower on Tregs in PBMC compared to the other tissue types (Figure S3). The activation landscape is also distinct in PBMC with significantly higher expression of GzmB on all T cell subsets and CD25 on CD4eff compared to the other tissue types. There was no significant difference in single checkpoint expression between the tissue types across the T cell subsets when split between patients who had SSA or not, except for TIGIT in CD8 normal tissue which was significantly higher in those who previously had SSA (Figure S5).

Tumour infiltrating lymphocytes in siNETs exhibit a more regulated co-expression phenotype compared to lymphocytes in normal tissue.

To further characterise the immune microenvironment of siNETs, we compared the expression of multiple checkpoints on $CD8^+$ and CD4eff T cells to interrogate the flow checkpoint phenotype overlap between the tissue types. The Treg population in siNETs was

too small for any meaningful co-expression analysis and was therefore excluded in this analysis. The immune markers with the most co-expression data were utilised including PD-1, CTLA-4, TIM-3, ICOS, GzmB and Ki67. Data from all samples of each tissue type was obtained using hierarchical gating strategy (Boolean) on FlowJo and subsequently analysed using a visualization software: 'Simplified Presentation of Incredibly Complex Evaluations' (SPICE) (31). We found a distinctive co-expression phenotype in PBMC compared to the other tissue types in both $CD8^+$ and CD4eff T cells (Figure 2A), while the differentiation of the immune landscape between normal tissue and tumour tissue was less apparent. The similarity in immune landscape between the normal tissue and that of the tumour was consistent across all of the samples obtained suggesting these expression patterns are representative of the tissue type, normal or tumour.

Unsupervised clustering of concatenated viable $CD8^+$ and CD4eff T cells in PBMC, normal tissue, primary and metastatic tumours revealed six T cell subpopulations with 1000 cell counts and more (Figure 2B), with clusters highlighting PBMC (red box) in $CD8^+$ (Pop3 and Pop4; Figure 2B) and CD4eff (Pop0 and Pop4; Figure 2B). Immune markers such as TIM-3 and 4-1BB with low expression on effector T cells were excluded in this analysis (Figure S4). The $CD8^+$ PBMC cluster of Pop3 and Pop4 and CD4eff PBMC cluster of Pop0 and Pop4 (Figure 2B) were distinctly different to the other tissue types with lower expression of checkpoint markers (PD-1, ICOS, CTLA-4), suggesting a less regulated immune tumour environment in the periphery. The GzmB expression on CD4eff PBMC cluster were high compared to tissue type, but varied on CD8. Visualization of the immune landscape by uniform manifold approximation and projection (UMAP) (32) dimension reduction likewise

revealed these cluster populations (blue) overlaying on each tissue type (orange) (Figure 2C). The metastatic clusters Pop2 and Pop5 having highest expression of checkpoint markers on CD8, while on CD4eff, the clusters Pop1 , Pop2 and Pop5 between the tissue types were similar. This mirrors the SPICE plots as depicted in Figure 2A with increased checkpoint expression of PD-1, ICOS and CTLA-4, while these checkpoint expression were similar on CD4eff. This demonstrates that in siNETs, the $CD8^+$ T cells are more regulated in metastatic tissue compared to other tissues and CD4eff.

In several solid tumours, combining checkpoint inhibitors, particularly the combination of -PD-1 and CTLA-4 inhibition, has improved outcomes compared PD-1 inhibition alone (8, 33-35), and many other checkpoint combination trials are underway (36). Since we found PD-1 to be highly expressed in the T cell subsets of siNETs, we analysed its co-expression with other checkpoint molecules to explore the rationale for combination therapy in this tumour type. PBMC were excluded in these analyses as shown to be distinctly different to tissue. Using PD-1 as a backbone, we found that $CD8^+$ tumour infiltrating lymphocytes had a significantly higher co-expression of PD-1/ICOS and PD-1/CTLA-4 (Figure 3A) and high levels of PD-1 expression (PD-1hi) compared to normal tissue (Figure 3B), suggesting a more regulated, chronically antigenic stimulated immune microenvironment in the tumour(37, 38). We also found that $CD8^+$ PD-1/GzmB(39). Similarly, we found a significantly higher CD4eff tumour infiltrating lymphocytes co-expression of PD-1/ICOS (Figure 3C) and PD-1hi (Figure 3D) compared to normal tissue. We also found was no significant difference in these co-expression populations between the tissue types across the T cell subsets when split between patients who had SSA or not, except for PD-1/ICOS in CD8 normal tissue which was significantly higher in those who previously did not have SSA (Figure S5). Taken together,

our data may suggest that we could use PD-1 as a checkpoint immunomodulator backbone in combination with CTLA-4 or ICOS to treat patients with siNET, although this needs to be tested in the clinical setting.

Evaluation of the geographical immune landscape shows that these tumours have poor infiltration by T cells.

Despite providing detailed insight into the molecular immune environment of siNET, flow cytometry does not allow the geographical immune landscape to be defined, and for this reason we also undertook an immunohistochemical (IHC) analysis. For all of the NET cases, FFPE tissue was obtained and stained using a multiplex IHC technique (23-25) to identify different T cell subsets. Single tissue sections were stained for cytokeratin, $CD8^+$, $CD4^+$ and $FoxP3^+$. For this analysis, $CD4^+$ T cells were not assessed as it was difficult to differentiate positive cells due to inadequate staining. The number of $CD8^+$ and Tregs were determined per mm^2 of tumour as described in the methods (Figure 4 A, B and D). Intra-tumoural T-cells were defined as those that fully in contact with tumour cells on all sides, whilst peri-tumoural T-cells were not fully in contact will tumour and within 100µm of the tumour edge. The analysis revealed that the majority of $CD8^+$ and Treg T cells subsets were peri-tumoural rather than intra-tumoural (Figure 4) as had been observed. This analysis indicated that in fact only 10.1% $CD8^+$ and 5.9% Tregs were intra-tumoural while 89.9% $CD8^+$ and 94.1% Tregs were peri-tumoural in both primary and metastatic tumours (Figure 4C).

For primary tumours (n=34) 10.3% $CD8^+$ and 3.2% Tregs were intra-tumoural while 89% $CD8^+$ and 96.8% Tregs were peri-tumoural. Furthermore, there was a significantly higher CD8/Treg ratio in peri-tumoural compared to intra-tumoural ($P = 0.018$), suggesting that not

only were there less intra-tumoural T cells, but the tumour microenvironment was more heavily regulated with lower intra-tumoural CD8/Treg ratio (Figure 4D).For metastases (n=28, comprising 25 mesenteric masses and 3 metastatic lymph nodes) 5.4% $CD8^+$ and 5.7% Tregs were intra-tumoural while 94.6% $CD8^+$ and 90.5% Tregs were peri-tumoural.

This indicates that there is a significantly lower number of intra-tumour T cells compared to peri-tumour in both primary and metastatic samples ($p = <0.001$). No significant relationships were identified between the numbers of peri-tumoural $CD8^+$ or Tregs and the clinical characteristics of the patient or tumour that we had collected (these included; gender, age, grade, Ki-67 index, metastasis or if they were on treatment somatostatin analogues, Table S1.). However, interestingly, when we looked into CD8/Treg ratio in primary and metastatic sites, there was a significantly higher peri-tumoural CD8/Treg ratio in metastatic sites ($p = <0.0001$) compared to primary sites, while there was no difference in intra-tumoural CD8/Treg ratio ($p = 0.57$). This is driven by significantly high number of peri-tumour Tregs in primary sites compared to metastases ($p = 0.0006$; Figure S6), and not peri-tumour or intra-tumour CD8s. The majority of our metastases were mesenteric metastases (69.4%), and with the mesentery being an organ that contains mainly fat, lymphatics and blood vessels, this may explain why there was a significantly higher number of peri-tumoural lymphocytes in this population. Additionally, there was one patient that had very high numbers of peri-tumoural T cells (both $CD8^+$ and Treg). This was a female patient 77 years of age who had no known metastases and was not on treatment with somatostatin analogues (Patient no.25 in Table S1.). This might be a tumour that is attracting a larger than normal T cell response but it is possible that this sample was taken from tumour that had

invaded a lymph node that was not obvious by IHC but resulted in high numbers of T cells present around the tumour tissue.

siNET have a low tumour mutational burden compared to other tumour types in TCGA cohort.

Tumour mutational burden (TMB) i.e. the number of somatic mutations per DNA megabase, can be estimated from next-generation sequencing assays and used as a proxy for neoantigen burden. Elevated TMB has been observed to be predictive of improved survival in patients receiving immune checkpoint inhibitors across differing tumour types, although TMB thresholds vary between cancer subtypes (40-42). The mutational rate of siNET genomes is known to be low, with few recurrent aberrations (43). We confirmed that patients with siNET had a low TMB with a median of 0.5 mutations/Mb (range 0.128-1.96). There was no correlation between the TMB and CD8/Treg ratio on IHC with a Spearman's Rho of -0.17 (95% confidence interval of -0.43 to 0.11; p = 0.22; Figure S8). We used the maftools package to compare the mutational burden of this dataset with TCGA cohorts and confirmed that TMB is low compared to other tumour types (Figure 5), and similar to the mutational load previously described for siNETs (44-46).

CDKN1b is the most frequently reported recurrent mutation in siNET, present in approximately 8% of patients (46). In our cohort, *CDKN1B* mutations had a similar frequency with 5 patient samples (9%) identified (Figure S7). Interestingly, in one patient, NET45 (patient no.39 in Table S1.), the *CDKN1B* mutation was identified in both metastatic samples but not in the primary tumour.

DISCUSSION

Immunotherapy is currently being explored in many tumour types with encouraging results, but there has only been relatively limited investigation of this modality for patients with NET. In this paper, we have characterised the immune-landscape in siNET with the aim of informing a rational approach for targeted immunotherapy in patients with NET.

We investigated the immune landscape in 40 siNET patients. The T cell subsets from the peripheral blood, primary tumour tissue, metastases and normal small intestinal tissue were analysed by multicolour flow cytometry. Analysis indicated that the primary tumours and metastatic tumours had a significantly lower ratio of $CD8^+$ to Tregs than in normal bowel tissue, while there was a significantly lower ratio of $CD4^+$ to Tregs than in blood. This signifies an imbalance between effector and Treg in a proliferating tumour, with a more inhibitory immune tumour microenvironment as compared with the normal bowel and suggests a potentially suppressive immune microenvironment within these tumours that may prevent tumour elimination.

Staining for co-inhibitory and co-stimulatory checkpoint molecules (CTLA-4, PD-1, TIM-3, TIGIT and ICOS, 4-1BB, OX-40, GITR respectively) on the T cell subsets showed that for all of the checkpoint molecules, their expression was highest on Tregs than in the other effector T cell subsets ($CD8^+$ and CD4eff), which is similar to what has been seen in other solid tumours (47, 48). This indicates that siNET might be uniquely targeted using immunomodulatory drugs directed towards depleting Tregs to shift the balance of the immune response in the tumours away from tumour tolerance and toward immune-mediated tumour elimination. Previous treatment with SSA did not seem to modulate the immune response in our cohort.

We had one patient who undergone PRRT which may affect the immune tumour microenvironment. However, number is too small to make any conclusion. We also identified that the immune checkpoint landscape had minimal flow phenotype overlap between PBMC and the rest of the tissue types. This is similar to previous published data (47) on flow cytometric analysis of PBMC and other tissue types.

High levels of PD-1 expression have previously been shown to identify tumour reactive T-cells (37, 49, 50) and are associated with distinct transcriptomic, phenotypic and functional properties (38, 51-53). Here, we demonstrate that these PD-1hi T cells were significantly more abundant in tumours compared to normal tissue, suggesting a chronically antigenic stimulated state. Interestingly, in one of the largest series of 64 siNETs, PD-1 expression on IHC was uncommon, with low levels of up to 1-20 cells/high power field which was limited to the stromal compartment (54), indicating the value of combining high dimensional flow cytometry in evaluating the immune tumour microenvironment of siNET. The observation that PD-1 effector tumour infiltrating lymphocytes were found to co-express multiple immune checkpoints, including CTLA-4 and ICOS suggest that combination therapy may be required to overcome resistance to monotherapy observed to date. Further functional experiments are needed to validate these findings and investigations exploring the therapeutic effect of these molecules, either alone or in conjunction with PD-1/PD-L1 blockade is therefore warranted. Our data suggests the potential use of combination immune checkpoint antibodies with anti-PD-1 therapy as a backbone, which warrants further investigations in future clinical trials. A better understanding of expression patterns and cell surface density of target checkpoint receptors across T cell subsets and tissue types is required to inform the most effective engineering of these antibodies and the

identification of the best combinatory immunomodulating therapies. This is pertinent, given that immunomodulatory antibodies may require antibody-dependent cellular cytotoxicity (ADCC) to enhance Treg depletion, in addition to stimulating or blocking immune checkpoint molecules (48, 55).

Immunohistochemical analysis of the tumours revealed that only 5-10% of $CD8^+$ and only 3-8% of Tregs are intra-tumoural while 89-95% and 89-97% are peri-tumoural respectively. Interestingly, not only were there higher numbers of peri-tumoural lymphocytes, but these were specifically significantly higher CD8/Treg compared to intra-tumoural. This 'excluded' phenotype suggests that the host immune system is able to mount a T cell-mediated immune response intrinsically and/or peripherally and yet is able to escape these responses by hampering T cell infiltration into the tumour microenvironment. There are several putative pathways that could explain this, including a possible role of extracellular matrix in promoting an immune exclusive phenotype, angiogenesis immune modulation via VEGFa, or oncogenic activation via WNT–β-catenin (56). Drugs targeting these pathways could be used in parallel with CPI to recruit these 'excluded' T cells into the tumour microenvironment. It will be important in future studies to elucidate the mechanism of T cell exclusion from these tumours to better understand this (54).

In this study, we have also shown that there was a high peri-tumoural CD8/Treg ratio in the metastatic sites. This is inverse to the published literature showing that there is a lower CD8/Treg ratio in metastatic site compared to primary site, likely due to immune evasion and escape, though in other tumour types like breast and colorectal cancers (57, 58). A plausible explanation may be due to the richness of lymphocytes in the mesentery due to

lymphatics and vasculature, as the majority of our metastases were mesenteric. Moreover, it is well described in the literature that the gut has a distinct immune microenvironment with Treg cells playing a critical role due to the continued diverse antigen exposure (59). Finally, PD-L1 which is used as a predictive biomarker in some tumour types, was not evaluated in our study and represents a potential limitation.

Previous groups have demonstrated a low TMB in siNET, with a median 0.1 – 1.098 variants per Mb (44-46, 60). TMB is an important determinant of clinical response to immune checkpoint blockade in most tumours (61) and therefore the low TMB found in siNETs may indicate less clinical benefit to immunotherapy with CPI. Additionally, da Silva and colleagues have shown a low IHC expression of PD-1 and PD-L1 in siNETs, together with low to moderate T cell infiltration, suggesting that response to single PD-1 or PD-L1 inhibitors may be modest, although this remains to be investigated. Therefore, it is vital to enhance tumour killing by combining with another CPI or with an anti-cancer drug that targets siNETs to prime immunity by causing cell death and release of tumour antigens.

For targeted immunotherapy to be effective in patients with siNET, it is critical to understand the immune landscape in which they exist. This work gives an insight into the inhibitory nature of the immune environment in these tumours and indicates that T cells are largely absent from within the tumour mass in siNET. It will be of great interest in future work to understand the reasons for the absence of T cells, primarily if there is an active exclusion mechanism at play or if the tumours are lacking sufficient neoantigens for the endogenous immune system to recognise the threat and act to eliminate them. We have, however, shown that there are potential immune-modulatory targets for siNETs in the form

of high checkpoint molecule expression on regulatory T cells that could provide a strategy for therapeutic intervention to tip the balance of the immune response to these tumours away from tumour tolerance and towards tumour elimination.

Acknowledgments

Funding: C Vesely: Neuroendocrine Tumor Research Foundation. T Meyer: University College London (UCL) CRUK and NIHR Experimental Cancer Medicine Centre Grant No. C12125/A15576, T Meyer: MRC award MR/M009033/1, T Meyer: UCL Hospitals NIHR Biomedical Research Centre.

549 **Table 1: Clinicopathological features of siNET cohort.**

550 Legend: SSA = Somatostatin analogues, Nil = Patient not on any treatment prior to sample collection,
551 PRRT = Peptide Receptor Radionuclide Therapy

	Number	%
Total	40	
Sex		
Male	23	57.5%
Female	17	42.5%
Age, median (range)	62	(27-85)
Metastatic site	30	75.0%
Ki-67 labelling index		
≤2% (Grade 1)	26	65.0%
>2 - 20% (Grade 2)	13	32.5%
>20% (Grade 3)	1	2.5%
Treatment		
Nil	15	37.5%
SSA	24	60.0%
PRRT	1	2.5%

552

Figure Legends

Figure 1: Effector/Treg ratio is significantly lower in tumour tissues and $CD8^+$ in metastatic tissue is significantly more regulated compared to other tissue types.

(A) The horizontal back bars indicate the median values for each compartment. The ratio of effectors to regulatory T cells was significantly lower in primary or metastatic tumour tissues compared to the normal tissue (CD8/Treg) and PBMCs (CD4eff/Treg). (B) Single level expression and co-expression of B7 and TNFR superfamily co-inhibitory and co-stimulatory molecules on T cell subsets were quantified by flow cytometry in matched peripheral blood mononuclear cells (PBMC), normal tissue, primary and metastatic tumour tissues obtained from all patients. Displayed is a heatmap depicting the mean percentage of $CD8^+$, CD4eff ($CD4^+$ $FoxP3^-$) and Tregs ($CD4^+$ $FoxP3^+$) cells expressing individual immune checkpoint molecules and proliferating markers in each tissue samples.

Figure 2: $CD8^+$ in metastatic tissue is more regulated compared to other tissue types. Co-expression of key B7 and TNFR superfamily co-inhibitory and co-stimulatory molecules on T cell subsets were quantified by flow cytometry with matched PBMCs, normal tissue and tumours from primary and metastatic sites. **(A)** SPICE analysis of all CD8+ and CD4eff T cells displaying the mean co-expression of checkpoint molecules across tissue types. **(B)** Unsupervised FlowSOM of CD8 and CD4eff clustering demonstrates that PBMC (red box) are distinctly different to other tissues types. **(C)** UMAP distribution of each FlowSOM CD8 and CD4eff populations (blue) on each tissue subtypes (orange).

Figure 3: Effector T cells in metastatic tissue is significantly more regulated compared to other tissue types. Co-expression of key B7 and TNFR superfamily coinhibitory and costimulatory molecules on T cell subsets were quantified using PD-1 as backbone by flow cytometry with matched normal tissue and tumours from primary and metastatic sites. **(A)** Graphs depict frequency of co-expression with PD-1 and ICOS, CTLA-4 and Granzyme B (GzmB) on $CD8^+$. Horizontal bars represent the mean; error bars show ± standard error of the mean (SEM). **(B)** Graphs depict frequency of high levels of PD-1 (PD-1hi) on $CD8^+$. Horizontal bars represent the mean; error bars show ± standard error of the mean (SEM). **(C)** Graphs depict frequency of co-expression with PD-1 and ICOS on CD4eff. Horizontal bars represent the mean; error bars show ± standard error of the mean (SEM). **(D)** Graphs depict frequency of high levels expression of PD-1 (PD-1hi) on CD4eff. Horizontal bars represent the mean; error bars show ± standard error of the mean (SEM). *, $P < 0.05$; **, $P < 0.005$; ***, $P < 0.0005$; ****, $P < 0.0001$.

Figure 4. The geographical immune landscape in siNET shows predominantly peri-tumoural T cells.

A and B. Immunohistochemistry (IHC) staining of siNET. T cell subsets stained are $CD8^+$ T cells (red), $CD4^+$ T cells (brown) and $FoxP3^+$ (blue) and tumour cells are stained for Cytokeratin (green). These images of two siNET show examples of a tumour with intra-tumoural T cells (A) or with mainly peri-tumoural T cells (B). Examples of intra-tumoural or peri-tumoural T cells are circled in black in figures 4A and B respectively. **C**. Plots of T cell counts per mm^2 showing that T cells are predominantly peri-tumoural rather than intra-tumoural in these tumours. **D**. Respective CD8/Treg ratio (Log10) in primary vs metastatic, peri-tumoural and intra-tumoural. Horizontal bars represent the mean; error bars show ± standard error of the mean (SEM). *, $P < 0.05$; ****, $P < 0.0001$.

Figure 5. SiNET mutational load

Figure shows a comparison of the siNET mutational load against 33 TCGA cohorts from the Multi-Center Mutation Calling in Multiple Cancers (MC3) (62) project.

REFERENCES

1. Pardoll DM. The blockade of immune checkpoints in cancer immunotherapy. Nat Rev Cancer. 2012;12(4):252-64.
2. Zou W, Chen L. Inhibitory B7-family molecules in the tumour microenvironment. Nature reviews Immunology. 2008;8(6):467-77.
3. Greenwald RJ, Freeman GJ, Sharpe AH. The B7 family revisited. Annual review of immunology. 2005;23:515-48.
4. Chen DS, Mellman I. Elements of cancer immunity and the cancer–immune set point. Nature. 2017;541(7637):321-30.
5. Topalian SL, Hodi FS, Brahmer JR, Gettinger SN, Smith DC, McDermott DF, et al. Safety, Activity, and Immune Correlates of Anti–PD-1 Antibody in Cancer. New England Journal of Medicine. 2012;366(26):2443-54.
6. Herbst RS, Soria J-C, Kowanetz M, Fine GD, Hamid O, Gordon MS, et al. Predictive correlates of response to the anti-PD-L1 antibody MPDL3280A in cancer patients. Nature. 2014;515(7528):563-7.
7. Hodi FS, O'Day SJ, McDermott DF, Weber RW, Sosman JA, Haanen JB, et al. Improved survival with ipilimumab in patients with metastatic melanoma. The New England journal of medicine. 2010;363(8):711-23.
8. Larkin J, Chiarion-Sileni V, Gonzalez R, Grob JJ, Rutkowski P, Lao CD, et al. Five-Year Survival with Combined Nivolumab and Ipilimumab in Advanced Melanoma. The New England journal of medicine. 2019;381(16):1535-46.
9. Dasari A, Shen C, Halperin D, Zhao B, Zhou S, Xu Y, et al. Trends in the Incidence, Prevalence, and Survival Outcomes in Patients With Neuroendocrine Tumors in the United States. JAMA oncology. 2017;3(10):1335-42.
10. Caplin ME, Pavel M, Ćwikła JB, Phan AT, Raderer M, Sedláčková E, et al. Lanreotide in metastatic enteropancreatic neuroendocrine tumors. The New England journal of medicine. 2014;371(3):224-33.
11. Sun W, Lipsitz S, Catalano P, Mailliard JA, Haller DG. Phase II/III study of doxorubicin with fluorouracil compared with streptozocin with fluorouracil or dacarbazine in the treatment of advanced carcinoid tumors: Eastern Cooperative Oncology Group Study E1281. J Clin Oncol. 2005;23(22):4897-904.
12. Pavel ME, Hainsworth JD, Baudin E, Peeters M, Horsch D, Winkler RE, et al. Everolimus plus octreotide long-acting repeatable for the treatment of advanced neuroendocrine tumours associated with carcinoid syndrome (RADIANT-2): a randomised, placebo-controlled, phase 3 study. Lancet. 2011;378(9808):2005-12.
13. Strosberg J, El-Haddad G, Wolin E, Hendifar A, Yao J, Chasen B, et al. Phase 3 Trial of (177)Lu-Dotatate for Midgut Neuroendocrine Tumors. The New England journal of medicine. 2017;376(2):125-35.
14. Strosberg JR, Mizuno N, Doi T, Grande E, Delord J-P, Shapira-Frommer R, et al. Efficacy and Safety of Pembrolizumab in Previously Treated Advanced Neuroendocrine Tumors: Results From the Phase 2 KEYNOTE-158 Study. Clinical Cancer Research. 2020:clincanres.3014.2019.
15. Capdevila J, Teule A, López C, García-Carbonero R, Benavent M, Custodio A, et al. 1157O A multi-cohort phase II study of durvalumab plus tremelimumab for the treatment of patients (pts) with advanced neuroendocrine neoplasms (NENs) of gastroenteropancreatic or lung origin: The DUNE trial (GETNE 1601). Annals of Oncology. 2020;31:S770-S1.
16. Yao JC, Strosberg J, Fazio N, Pavel ME, Bergsland E, Ruszniewski P, et al. Spartalizumab in metastatic, well/poorly-differentiated neuroendocrine neoplasms. Endocrine-related cancer. 2021.
17. Patel SP, Othus M, Chae YK, Giles FJ, Hansel DE, Singh PP, et al. A Phase II Basket Trial of Dual Anti-CTLA-4 and Anti-PD-1 Blockade in Rare Tumors (DART SWOG 1609) in Patients with Nonpancreatic Neuroendocrine Tumors. Clinical cancer research : an official journal of the American Association for Cancer Research. 2020;26(10):2290-6.
18. Takkenkamp TJ, Jalving M, Hoogwater FJH, Walenkamp AME. The immune tumour microenvironment of neuroendocrine tumours and its implications for immune checkpoint inhibitors. Endocrine-related cancer. 2020;27(9):R329-r43.
19. Rindi G, Klöppel G, Alhman H, Caplin M, Couvelard A, de Herder WW, et al. TNM staging of foregut (neuro)endocrine tumors: a consensus proposal including a grading system. Virchows Archiv. 2006;449(4):395-401.

20. Wick DA, Webb JR, Nielsen JS, Martin SD, Kroeger DR, Milne K, et al. Surveillance of the Tumor Mutanome by T Cells during Progression from Primary to Recurrent Ovarian Cancer. Clinical Cancer Research. 2014;20(5):1125.
21. Roncador G, Brown PJ, Maestre L, Hue S, Martínez-Torrecuadrada JL, Ling KL, et al. Analysis of FOXP3 protein expression in human CD4+CD25+ regulatory T cells at the single-cell level. European journal of immunology. 2005;35(6):1681-91.
22. Banham AH, Lyne L, Scase TJ, Blacklaws BA. Monoclonal antibodies raised to the human FOXP3 protein can be used effectively for detecting Foxp3(+) T cells in other mammalian species. Veterinary immunology and immunopathology. 2009;127(3-4):376-81.
23. Marafioti T, Paterson JC, Ballabio E, Reichard KK, Tedoldi S, Hollowood K, et al. Novel markers of normal and neoplastic human plasmacytoid dendritic cells. Blood. 2008;111(7):3778-92.
24. Akarca AU, Shende VH, Ramsay AD, Diss T, Pane-Foix M, Rizvi H, et al. BRAF V600E mutation-specific antibody, a sensitive diagnostic marker revealing minimal residual disease in hairy cell leukaemia. Br J Haematol. 2013;162(6):848-51.
25. Marafioti T, Jones M, Facchetti F, Diss TC, Du MQ, Isaacson PG, et al. Phenotype and genotype of interfollicular large B cells, a subpopulation of lymphocytes often with dendritic morphology. Blood. 2003;102(8):2868-76.
26. Obeid JM, Wages NA, Hu Y, Deacon DH, Slingluff CL, Jr. Heterogeneity of CD8(+) tumor-infiltrating lymphocytes in non-small-cell lung cancer: impact on patient prognostic assessments and comparison of quantification by different sampling strategies. Cancer immunology, immunotherapy : CII. 2017;66(1):33-43.
27. Garcia M, Juhos S, Larsson M, Olason P, Martin M, Eisfeldt J, et al. Sarek: A portable workflow for whole-genome sequencing analysis of germline and somatic variants [version 2; peer review: 2 approved]. F1000Res. 2020;9(63).
28. Shyr C, Tarailo-Graovac M, Gottlieb M, Lee JJY, van Karnebeek C, Wasserman WW. FLAGS, frequently mutated genes in public exomes. BMC Medical Genomics. 2014;7(1):64.
29. Martínez-Lostao L, Anel A, Pardo J. How Do Cytotoxic Lymphocytes Kill Cancer Cells? Clinical Cancer Research. 2015;21(22):5047.
30. Boyman O, Sprent J. The role of interleukin-2 during homeostasis and activation of the immune system. Nature Reviews Immunology. 2012;12(3):180-90.
31. Roederer M, Nozzi JL, Nason MC. SPICE: Exploration and analysis of post-cytometric complex multivariate datasets. Cytometry Part A. 2011;79A(2):167-74.
32. Becht E, McInnes L, Healy J, Dutertre C-A, Kwok IWH, Ng LG, et al. Dimensionality reduction for visualizing single-cell data using UMAP. Nature Biotechnology. 2019;37(1):38-44.
33. Hellmann MD, Paz-Ares L, Bernabe Caro R, Zurawski B, Kim SW, Carcereny Costa E, et al. Nivolumab plus Ipilimumab in Advanced Non-Small-Cell Lung Cancer. The New England journal of medicine. 2019;381(21):2020-31.
34. Overman MJ, Lonardi S, Wong KYM, Lenz HJ, Gelsomino F, Aglietta M, et al. Durable Clinical Benefit With Nivolumab Plus Ipilimumab in DNA Mismatch Repair-Deficient/Microsatellite Instability-High Metastatic Colorectal Cancer. Journal of clinical oncology : official journal of the American Society of Clinical Oncology. 2018;36(8):773-9.
35. Motzer RJ, Tannir NM, McDermott DF, Arén Frontera O, Melichar B, Choueiri TK, et al. Nivolumab plus Ipilimumab versus Sunitinib in Advanced Renal-Cell Carcinoma. The New England journal of medicine. 2018;378(14):1277-90.
36. Meric-Bernstam F, Larkin J, Tabernero J, Bonini C. Enhancing anti-tumour efficacy with immunotherapy combinations. The Lancet. 2021;397(10278):1010-22.
37. Gros A, Robbins PF, Yao X, Li YF, Turcotte S, Tran E, et al. PD-1 identifies the patient-specific CD8(+) tumor-reactive repertoire infiltrating human tumors. J Clin Invest. 2014;124(5):2246-59.
38. Thommen DS, Koelzer VH, Herzig P, Roller A, Trefny M, Dimeloe S, et al. A transcriptionally and functionally distinct PD-1(+) CD8(+) T cell pool with predictive potential in non-small-cell lung cancer treated with PD-1 blockade. Nat Med. 2018.
39. Ghorani E, Reading JL, Henry JY, Massy MRd, Rosenthal R, Turati V, et al. The T cell differentiation landscape is shaped by tumour mutations in lung cancer. Nature Cancer. 2020;1(5):546-61.
40. Hellmann MD, Ciuleanu TE, Pluzanski A, Lee JS, Otterson GA, Audigier-Valette C, et al. Nivolumab plus Ipilimumab in Lung Cancer with a High Tumor Mutational Burden. The New England journal of medicine. 2018;378(22):2093-104.

41. Samstein RM, Lee CH, Shoushtari AN, Hellmann MD, Shen R, Janjigian YY, et al. Tumor mutational load predicts survival after immunotherapy across multiple cancer types. Nat Genet. 2019;51(2):202-6.
42. Fabrizio DA, George TJ, Jr., Dunne RF, Frampton G, Sun J, Gowen K, et al. Beyond microsatellite testing: assessment of tumor mutational burden identifies subsets of colorectal cancer who may respond to immune checkpoint inhibition. Journal of gastrointestinal oncology. 2018;9(4):610-7.
43. Samsom KG, Veenendaal LMv, Valk GD, Vriens MR, Tesselaar MET, Berg JGvd. Molecular prognostic factors in small-intestinal neuroendocrine tumours. Endocrine Connections. 2019;8(7):906-22.
44. Hao D, Wang L, Di LJ. Distinct mutation accumulation rates among tissues determine the variation in cancer risk. Sci Rep. 2016;6:19458.
45. Banck MS, Kanwar R, Kulkarni AA, Boora GK, Metge F, Kipp BR, et al. The genomic landscape of small intestine neuroendocrine tumors. J Clin Invest. 2013;123(6):2502-8.
46. Francis JM, Kiezun A, Ramos AH, Serra S, Pedamallu CS, Qian ZR, et al. Somatic mutation of CDKN1B in small intestine neuroendocrine tumors. Nat Genet. 2013;45(12):1483-6.
47. Wong YNS, Joshi K, Khetrapal P, Ismail M, Reading JL, Sunderland MW, et al. Urine-derived lymphocytes as a non-invasive measure of the bladder tumor immune microenvironment. The Journal of experimental medicine. 2018;215(11):2748-59.
48. Arce Vargas F, Furness AJS, Litchfield K, Joshi K, Rosenthal R, Ghorani E, et al. Fc Effector Function Contributes to the Activity of Human Anti-CTLA-4 Antibodies. Cancer cell. 2018;33(4):649-63.e4.
49. McGranahan N, Furness AJ, Rosenthal R, Ramskov S, Lyngaa R, Saini SK, et al. Clonal neoantigens elicit T cell immunoreactivity and sensitivity to immune checkpoint blockade. Science. 2016;351(6280):1463-9.
50. Inozume T, Hanada K, Wang QJ, Ahmadzadeh M, Wunderlich JR, Rosenberg SA, et al. Selection of CD8+PD-1+ lymphocytes in fresh human melanomas enriches for tumor-reactive T cells. J Immunother. 2010;33(9):956-64.
51. Thommen DS, Schreiner J, Muller P, Herzig P, Roller A, Belousov A, et al. Progression of Lung Cancer Is Associated with Increased Dysfunction of T Cells Defined by Coexpression of Multiple Inhibitory Receptors. Cancer immunology research. 2015;3(12):1344-55.
52. Zappasodi R, Budhu S, Hellmann MD, Postow MA, Senbabaoglu Y, Manne S, et al. Non-conventional Inhibitory CD4. Cancer cell. 2018;33(6):1017-32.e7.
53. Reading JL, Galvez-Cancino F, Swanton C, Lladser A, Peggs KS, Quezada SA. The function and dysfunction of memory CD8(+) T cells in tumor immunity. Immunol Rev. 2018;283(1):194-212.
54. da Silva A, Bowden M, Zhang S, Masugi Y, Thorner AR, Herbert ZT, et al. Characterization of the Neuroendocrine Tumor Immune Microenvironment. Pancreas. 2018;47(9):1123-9.
55. Simpson TR, Li F, Montalvo-Ortiz W, Sepulveda MA, Bergerhoff K, Arce F, et al. Fc-dependent depletion of tumor-infiltrating regulatory T cells co-defines the efficacy of anti-CTLA-4 therapy against melanoma. The Journal of experimental medicine. 2013;210(9):1695-710.
56. Galon J, Bruni D. Approaches to treat immune hot, altered and cold tumours with combination immunotherapies. Nature Reviews Drug Discovery. 2019;18(3):197-218.
57. Ogiya R, Niikura N, Kumaki N, Bianchini G, Kitano S, Iwamoto T, et al. Comparison of tumor-infiltrating lymphocytes between primary and metastatic tumors in breast cancer patients. Cancer science. 2016;107(12):1730-5.
58. Jakubowska K, Koda M, Kisielewski W, Kańczuga-Koda L, Famulski W. Tumor-infiltrating lymphocytes in primary tumors of colorectal cancer and their metastases. Experimental and therapeutic medicine. 2019;18(6):4904-12.
59. Whibley N, Tucci A, Powrie F. Regulatory T cell adaptation in the intestine and skin. Nature Immunology. 2019;20(4):386-96.
60. Samsom KG, Levy S, van Veenendaal LM, Roepman P, Kodach LL, Steeghs N, et al. Driver mutations occur frequently in metastases of well-differentiated small intestine neuroendocrine tumours. Histopathology. 2021;78(4):556-66.
61. Alexandrov LB, Nik-Zainal S, Wedge DC, Aparicio SAJR, Behjati S, Biankin AV, et al. Signatures of mutational processes in human cancer. Nature. 2013;500(7463):415-21.
62. Ellrott K, Bailey MH, Saksena G, Covington KR, Kandoth C, Stewart C, et al. Scalable Open Science Approach for Mutation Calling of Tumor Exomes Using Multiple Genomic Pipelines. Cell Systems. 2018;6(3):271-81.e7.

Figure 1

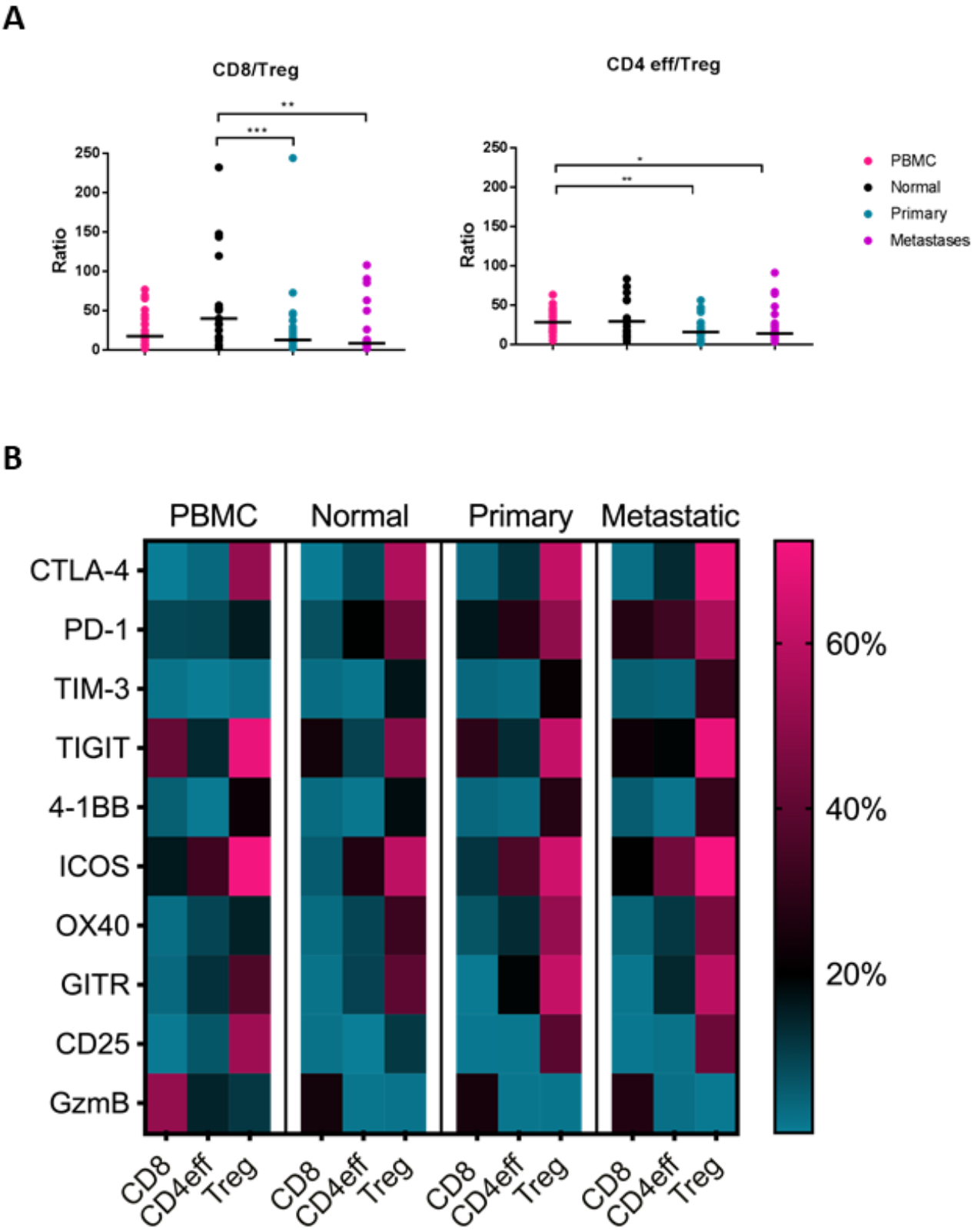

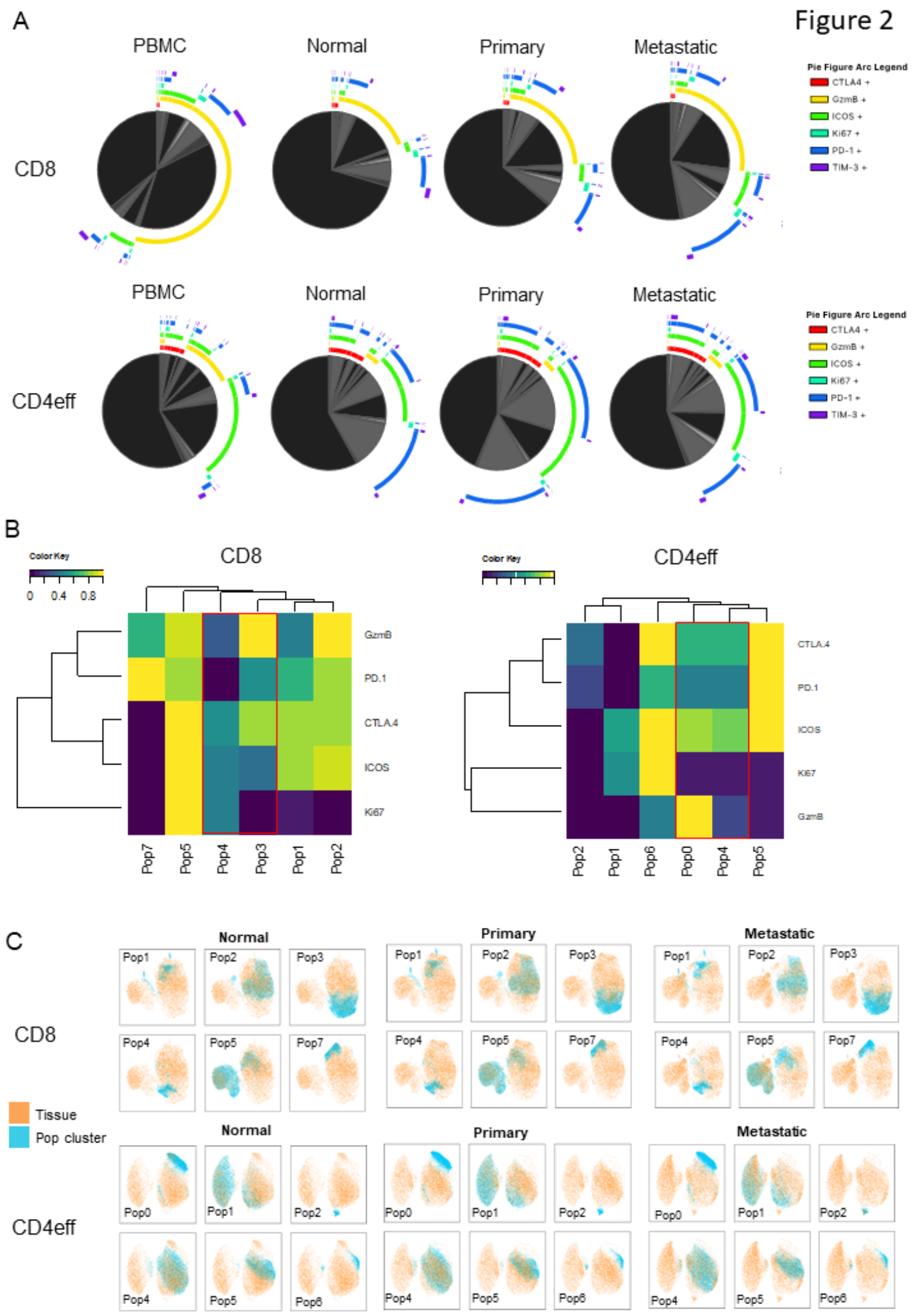

Figure 3

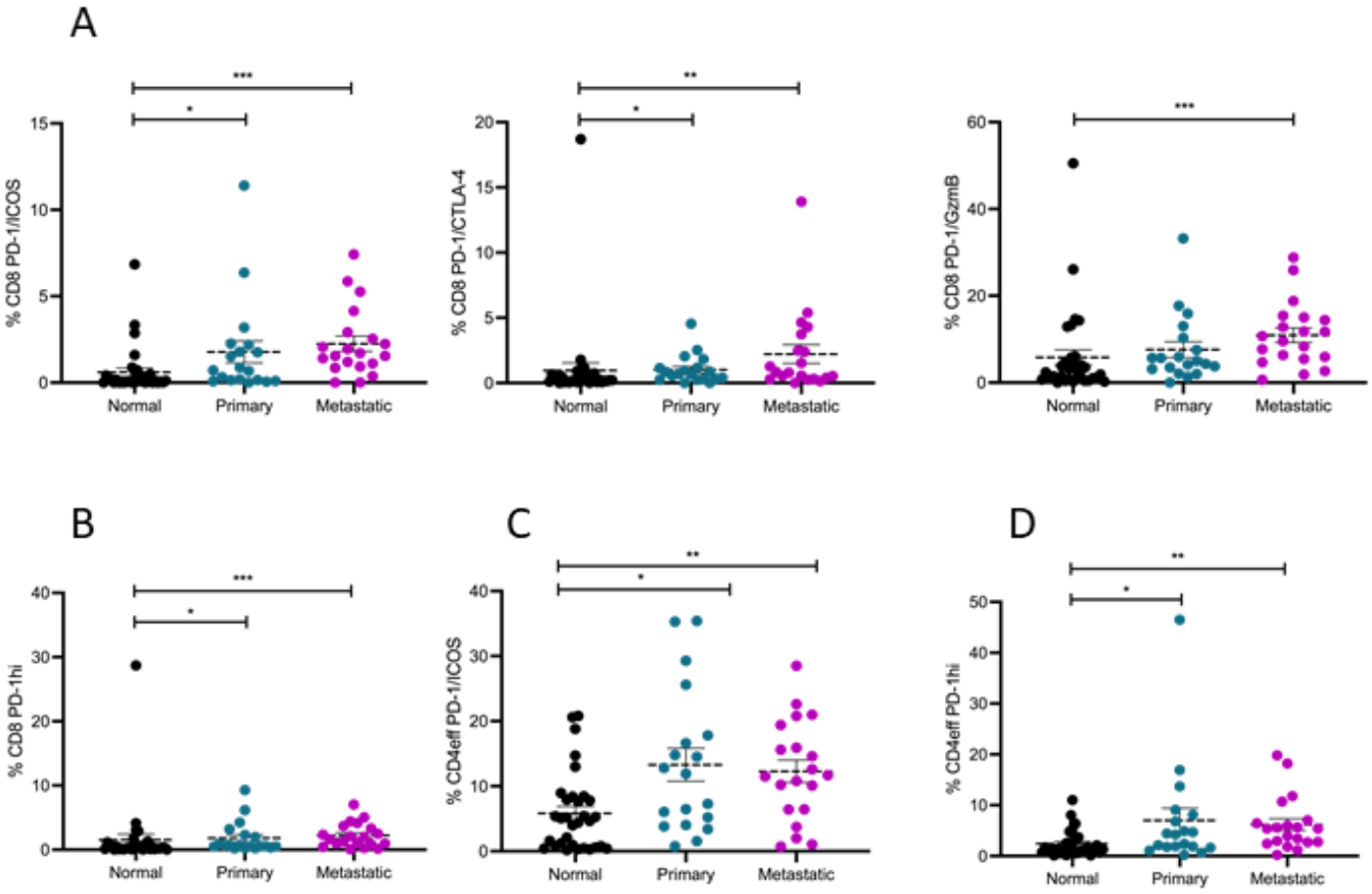

Figure 4

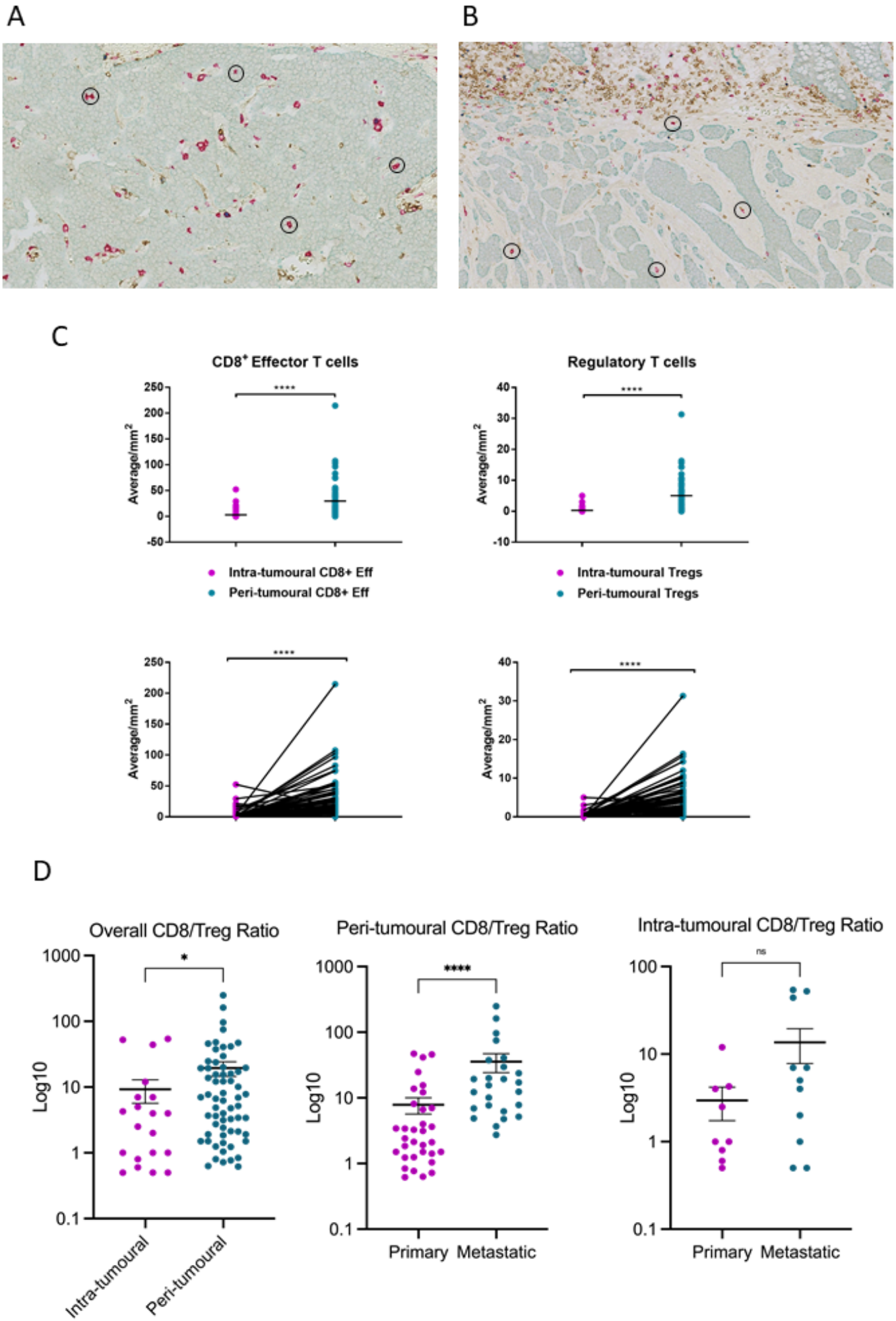

Figure 5